JOC The Journal of Organic Chemistry

Article

pubs.acs.org/joc

Acid–Base Properties of a Freebase Form of a Quadruply Ring-Fused Porphyrin—Stepwise Protonation Induced by Rigid Ring-Fused Structure

Yuta Saegusa,[†] Tomoya Ishizuka,[*,†] Yoshihito Shiota,[‡] Kazunari Yoshizawa,[‡] and Takahiko Kojima[*,†]

[†]Department of Chemistry, Graduate School of Pure and Applied Sciences, University of Tsukuba, 1-1-1 Tennoudai, Tsukuba, Ibaraki 305-8571, Japan

[‡]Institute for Materials Chemistry and Engineering, Kyushu University, Motooka, Nishi-Ku, Fukuoka 819-0395, Japan

Supporting Information

ABSTRACT: We report herein unique stepwise protonation at inner imino-nitrogen atoms of a freebase derivative of a quadruply fused porphyrin (H_2QFP), which has been newly synthesized. H_2QFP has been revealed to have the two inner NH protons on the two nonfused pyrroles by X-ray diffraction analysis and ^{1}H NMR spectroscopy. The first protonation at one of the two imino-nitrogen atoms of the fused pyrroles smoothly proceeds with trifluoroacetic acid (TFA) in CH_2Cl_2 and the equilibrium constant (K_1) of the protonation has been determined to be $(1.3 \pm 0.1) \times 10^5$ M^{-1}. In contrast, the second protonation at the other imino-nitrogen atom is hard to occur unless a large excess amount of TFA is used, as reflected on a much smaller equilibrium constant, $K_2 = 7.3 \pm 0.3$ M^{-1}. The stepwise protonation is ascribed to the structural rigidity caused by the ring fusion and the resultant steric repulsion among inner NH atoms of the diprotonated form. Electrochemical studies have revealed that protonation at the pyrrole nitrogen atoms caused positive shifts of the reduction potentials of the QFP derivatives. In addition, the ESR spectrum of the electrochemically one-electron-reduced monoprotonated QFP derivative showed well-resolved hyperfine splitting to represent its unsymmetrical electronic structure due to the monoprotonation.

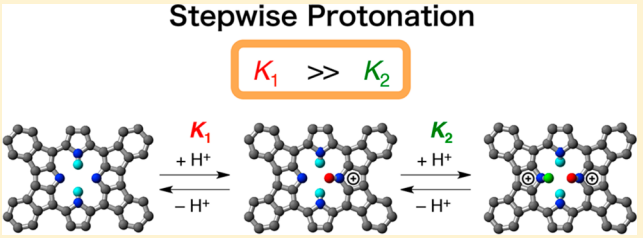

INTRODUCTION

Freebase porphyrins have attracted much attention not only for versatile utility as ligands for various metal ions,[1] but also due to the interest in the unique electrochemical properties.[2] For instance, inspired by the fact that pheophytin, the freebase form of chlorophyll, is utilized as the first electron acceptor from the photoexcited special pair in the reaction center of photosystem II,[3] freebase porphyrins have been used as an electron acceptor in photoinduced electron-transfer systems with use of zinc(II)-porphyrinato complexes as electron donors.[4] Freebase porphyrins also can function as weak bases ($pK_a = \sim 4$),[5] whereas they also behave as weak acids to release one proton.[6] Porphyrins are known to selectively undergo diprotonation and thus the intermediate monoprotonated state is difficult to be detected.[5,7−9] Protonation of a freebase porphyrin has been known to exert strong impacts on shape and electronic structure of the π-conjugated system, as represented by conformational deformation of the ring structure,[5c,10] red shifts of the absorption bands,[11,12] and elevation of the redox potentials.[2c,13] Diprotonated porphyrins also have attracted interest due to their self-aggregation induced by protonation.[14,15] In addition, the elevated reduction potentials of diprotonated porphyrins enable them to act as more efficient electron acceptors.[16]

Recently, a lot of efforts have been dedicated to synthesis and characterization of novel π-expanded porphyrins having ring-fused structures at the periphery.[17−27] Among them, the derivatives having fused five-membered rings have attracted attention due to the interest in their unique aromaticity.[28−32] However, effects of the ring fusion on properties of the freebase derivatives of ring-fused porphyrins, such as acid–base properties, have yet to be explored. We have recently reported the synthesis of a zinc(II) complex of a quadruply fused porphyrin (Zn^{II}QFP), and the characteristics and supramolecular interaction with fullerenes.[33] The QFP ligand in Zn^{II}QFP shows a rhombically distorted structure; that is, the interatomic distance between the two inner nitrogen atoms of the fused pyrroles is shortened, whereas that between the two inner nitrogen atoms of the nonfused pyrroles is elongated, relative to those of Zn^{II}TPP (TPP = tetraphenylporphyrin).[33a] Consequently, the mean bond distance between the nitrogen atoms and the central Zn^{II} ion is elongated in comparison to that of Zn^{II}TPP; as a result of the elongation, the Lewis acidity of the central Zn^{II} ion is enhanced.[33b,c] Additionally, the π-conjugation circuit of QFP expands to the fused *meso*-aryl groups and the properties of QFP, such as redox potentials, are

Received: October 5, 2016
Published: December 14, 2016

ACS Publications © 2016 American Chemical Society

DOI: 10.1021/acs.joc.6b02419
J. Org. Chem. 2017, 82, 322−330

highly sensitive to the substituents at the fused aryl groups.[33b] The expansion of the π-conjugation circuit causes contribution of antiaromatic circuits to the magnetic properties of QFP.[33b] Concerning the protonation of freebase ring-fused porphyrins, however, no detailed investigation has been made to elucidate impacts of the protonation on the characteristics including electronic structures and redox potentials. Herein, we describe synthesis and characterization of a novel freebase QFP derivative and report the stepwise protonation behavior (Scheme 1). Furthermore, the unsymmetrical structure of the monoprotonated QFP derivative has been elucidated by an ESR spectrum of its electrochemically 1e$^-$-reduced species.

Scheme 1

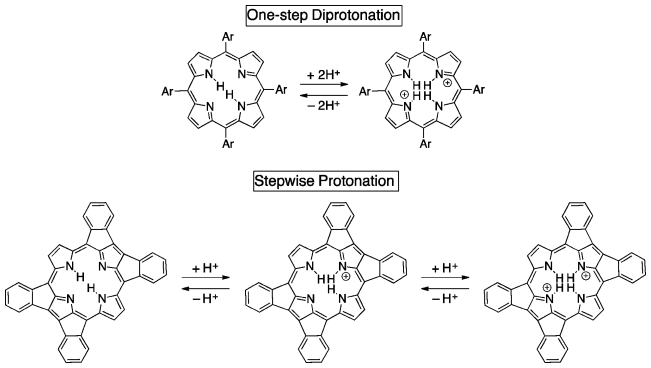

RESULTS AND DISCUSSION

Synthesis and Spectroscopic Characterization. Syntheses of freebase QFP derivatives can be performed by treatment of the Zn^{II} complex (**1**)[33] with TFA (= trifluoroacetic acid) in $CHCl_3$ (Scheme 2). Herein, we chose the *tert*-butyl (*t*-Bu) derivative of QFP, which has four *t*-Bu groups at the *para*-position of the fused *meso*-aryl groups, because the freebase form of the *t*-Bu-QFP, **2**, is exceptionally soluble in $CHCl_3$ among the QFP derivatives synthesized so far. Characterization of **2** was performed by ^{1}H NMR and UV−vis spectroscopies, MALDI-TOF-MS spectrometry, elemental analysis,[34] and single-crystal X-ray crystallography (see below).

Scheme 2

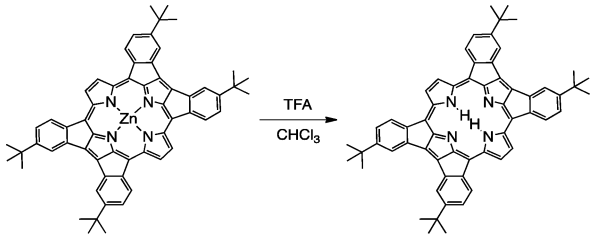

In the ^{1}H NMR spectrum of **2** in $CDCl_3$, only six signals were observed, reflecting the D_{2h} symmetry (Figure 1a). Four signals observed in the range of δ 6.7−7.6 ppm were derived from the pyrrole β-Hs and the hydrogen atoms of the fused aryl groups. A broad signal observed at 4.98 ppm was assigned to the inner NH protons. To confirm the exchangeability of the NH protons, an aliquot of D_2O was added to the solution. Then the ^{1}H NMR signal at 4.98 ppm gradually diminished, and simultaneously, the doublet signal at 7.53 ppm (J = 1.6 Hz;

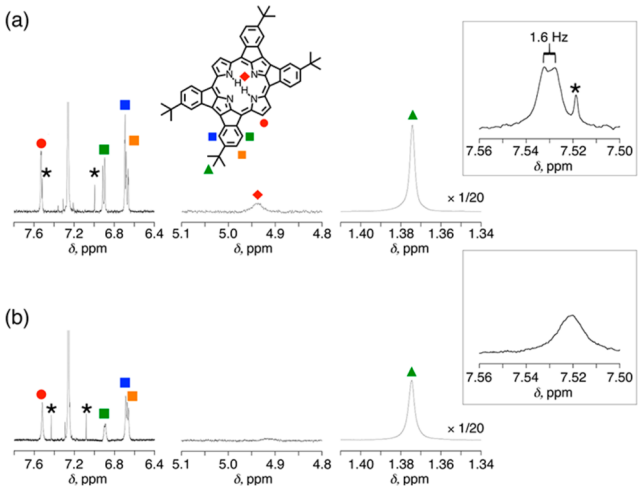

Figure 1. ^{1}H NMR spectra of **2** in $CDCl_3$ at 298 K before (a) and after addition of an aliquot of D_2O (b). Insets: Magnified spectra in the range of 7.52−7.58 ppm. Asterisks (*) denote the satellite signal of chloroform.

Figure 1a, inset) became a singlet (Figure 1b). This indicates that the signal at 7.55 ppm is ascribable to the pyrrole-β protons, coupled with the inner NH protons observed at 4.98 ppm. Therefore, the inner NH protons were revealed to localize at the nonfused pyrroles (see below).[35,36] Additionally, the inner NH signal was highly downfield shifted in comparison to that of the corresponding TPP derivative, tetrakis(*p*-*t*-Bu-phenyl)-porphyrin (**3**; Chart 1):[37] δ_{NH} −2.77 ppm. The

Chart 1

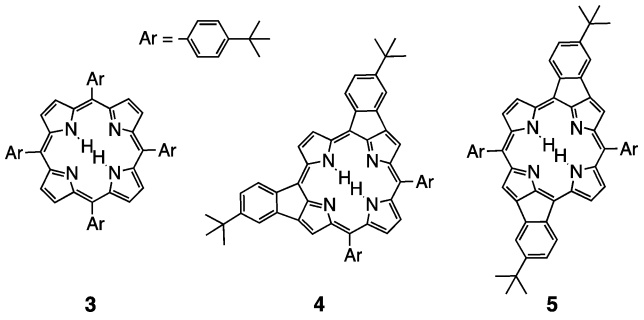

downfield shift observed for the NH signal of **2** can be accounted for by the weak aromatic currents of **2** and strong hydrogen bonding of the inner NH protons with the vicinal imine nitrogen atoms in **2**. As described previously,[30a,33b] the shielding effect on the inside of QFP is weak due to contribution of the antiaromatic ring currents. In fact, the NICS(1) value[38] of **2** (−5.9) is more positive than that of **3** (NICS(1): −13). On the other hand, the interatomic distances between adjacent nitrogen atoms of **2** are shorter than those of **3** (see below). As a result of the short distances, strong hydrogen bonding should be formed between inner NH protons and imine nitrogen atoms in **2**. Supporting this assumption, the stretching band of the inner N−H bonds (ν_{NH}) for **2** was observed at 3134 cm^{-1} in the IR spectrum, which was low-energy shifted relative to that for **3** (ν_{NH} = 3315 cm^{-1}).[39] The low-energy shift of the stretching band derives from the strong hydrogen bonding of the inner NH protons with the imine-nitrogen atoms in **2**.[40] As mentioned above, the

DOI: 10.1021/acs.joc.6b02419
J. Org. Chem. 2017, 82, 322−330

strong hydrogen bonding of **2** also contributes to the downfield shift of the ^{1}H NMR signal of the inner NH protons.

Crystal Structure of 2. A single crystal of **2** suitable for X-ray diffraction analysis was obtained with recrystallization from the solution in $CHCl_3$ with vapor diffusion of CH_3CN as a poor solvent. The crystal system is monoclinic with the space group of $P2_1/n$ and the asymmetric unit includes three and a half molecules of **2** and four molecules of $CHCl_3$ as cocrystallized solvent molecules, which are highly disordered and thus deleted with the SQUEEZE program.[41] The ORTEP drawings of one of the independent molecules of **2** are shown in Figure 2.

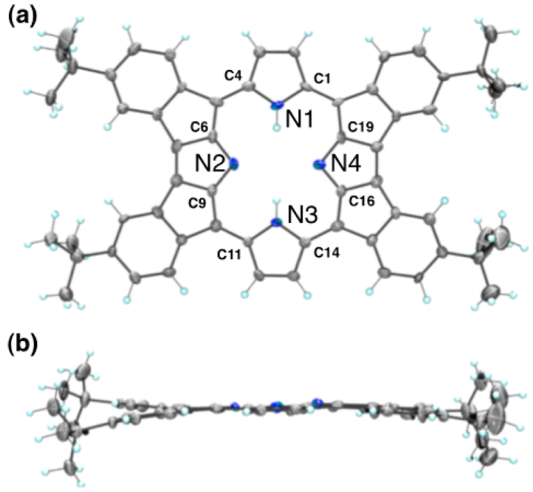

Figure 2. ORTEP drawings of the crystal structure of **2**: (a) top and (b) side views with the thermal ellipsoids of 40% probability.

Compound **2** is almost planar and the mean deviation from the least-squares plane consisting of 48 atoms including the fused *meso*-aryl groups is 0.089 Å. Reflecting the planarity, the molecules of **2** formed a $\pi-\pi$ stacking pentamer (Figure S3) and the pentamer was surrounded by another molecule of **2** due to the CH/π interaction between the *t*-Bu groups and the porphyrin π-plane. The porphyrin core of **2** was rhombically distorted due to the ring-fusion, similarly to Zn^{II}QFP derivatives.[33] The interatomic distances between two nitrogen atoms diagonally positioned are 4.615(9) Å for N1···N3 and 3.374(7) Å for N2···N4; that is, contracted between the fused pyrroles, whereas expanded between the nonfused pyrroles. Additionally, the bond angles of Cα–N–Cα of pyrroles showed characteristic difference between the fused and nonfused pyrroles; that is, those of nonfused pyrroles ($\angle$C1–N1–C4 = 111.9(7)° and $\angle$C11–N3–C14 = 112.3(7)°) were wider than those of fused ones ($\angle$C6–N2–C9 = 100.3(6)° and $\angle$C16–N4–C19 = 100.8(7)°). The wider bond angle of Cα–N–Cα over 109° in porphyrin pyrrole rings generally indicates that the inner NH proton localizes on the pyrrole, whereas the narrower one below 105° does that the pyrrole is in the imino form.[42,43] Therefore, consistent with the results of the ^{1}H NMR spectroscopy (see above), the two inner NH protons localize at the nonfused pyrroles in the solid state as well as in solution.

DFT Calculations on 2. To elucidate the difference in stability between two NH tautomers of **2**, we performed DFT calculations on them (Figure 3) at the B3LYP/6-31G** level of theory. As a result, the tautomer A, which has the two inner NH protons on the nonfused pyrroles, is more stable by 12.5 kcal mol^{-1} than the tautomer B, in which the two inner NH

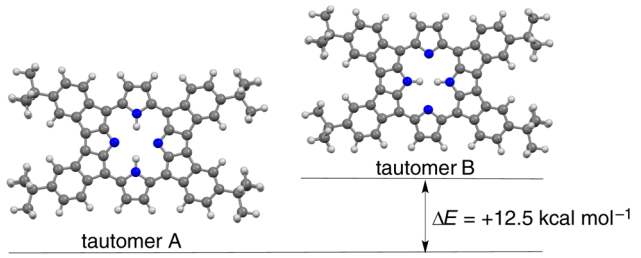

Figure 3. DFT-optimized structures of the two tautomers A (left) and B (right) at the B3LYP/6-31G** level of theory.

protons are located on the fused pyrroles. The large difference in stability is probably derived from the two factors: the steric repulsion between the two closely located inner NH protons in tautomer B and the resonance stabilization in tautomer A. The N2···N4 distance (3.374(7) Å), observed in the crystal structure, is significantly shorter than the sum of two N–H bond lengths (ca. 1.0 Å)[44] and van der Waals radii of two hydrogen atoms (ca. 1.2 Å);[45] that is, 2 × 1.0 + 2 × 1.2 = 4.4 Å. Actually, the DFT-optimized structure of tautomer B exhibits deviation of the two inner NH protons from the QFP mean plane to avoid steric repulsion. In addition, for tautomer B, only 18π aromatic circuits can be drawn, whereas tautomer A has 25 kinds of resonance structures of 18π–30π circuits including 20π and 24π antiaromatic circuits (Figure S4). The possible contribution of various resonance structures also assists the stability of the tautomer A.

Basicities of Ring-Fused Porphyrins. The basicity of the imino-nitrogen atoms of the fused pyrroles in **2** was explored by UV–vis titration with TFA as an acid in CH_2Cl_2 at 298 K (Figure 4). The absorption spectrum of **2** (1.5×10^{-5} M) in CH_2Cl_2 exhibited a Soret-like band at 604 nm and Q-like bands at 865, 817, and 744 nm; addition of TFA up to 1.5×10^{-4} M caused weakening and broadening of the Soret-like band, accompanying an isosbestic point at 428 nm (Figure 4a). Further addition of TFA brought rise and red shift of the Soret-like band with showing an isosbestic point at 415 nm (Figure 4b). Therefore, it is clarified that **2** undergoes two-step protonation (Scheme 3). Analysis of the absorbance change at 601 nm for the first step and that at 631 nm for the second step allowed us to determine the equilibrium constant of each step (insets of Figure 4): $K_1 = (1.3 \pm 0.1) \times 10^5$ M^{-1} and $K_2 = 7.3 \pm 0.3$ M^{-1}. As the equilibrium constants indicate, the second protonation is very difficult relative to the first protonation. As a piece of evidence to support that the first equilibrium process observed in the UV–vis titration was monoprotonation of **2**, a Job's plot was made with changing the concentration of **2** and TFA (Figure S5). The Job's plot clearly indicates that the binding process between **2** and TFA is a 1:1 process, i.e., monoprotonation. To compare the equilibrium constants of the protonation, UV–vis titrations of the TPP derivative, **3**, and *cis*- and *trans*-doubly fused porphyrins (**4** and **5**; Chart 1) with TFA in CH_2Cl_2 were also performed (Figure S6–S8). The equilibrium constants obtained are summarized in Table 1. Compound **3** exhibited one-step diprotonation, as previously reported,[5] and the overall formation constant, β (= $K_1 \times K_2$), was determined to be $(1.0 \pm 0.3) \times 10^{10}$ M^{-2}. Doubly fused **4** and **5** exhibited two-step protonation, similarly to **2**, and the Job's plots suggested that the first equilibrium processes were also based on the monoprotonation (Figure S9). The first protonation constants, K_1, of **2**, **4**, and **5** are in the same order of 10^5 M^{-1}, which corresponds to the square root of

DOI: 10.1021/acs.joc.6b02419
J. Org. Chem. 2017, 82, 322–330

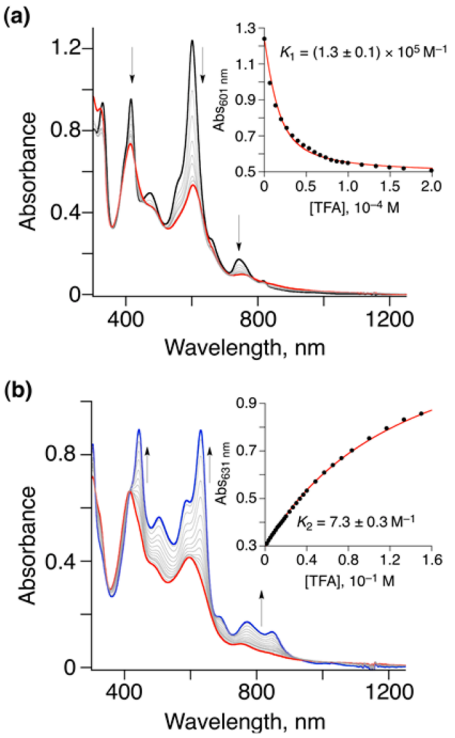

Figure 4. UV−vis spectral changes of **2** (1.5×10^{-5} M) in CH_2Cl_2 upon addition of TFA at 298 K. The concentration ranges of TFA are $0-1.5 \times 10^{-4}$ M (a) and $5.0 \times 10^{-3} - 0.15$ M (b). The red traces in both (a) and (b) indicate the spectrum of the monoprotonated form. Insets: the absorbance changes at 601 nm for (a) and 631 nm for (b) and the fitting curves to obtain the equilibrium constants.

Scheme 3

$$H_2P + H^+ \underset{}{\overset{K_1}{\rightleftharpoons}} H_3P^+ \qquad K_1 = \frac{[H_3P^+]}{[H_2P][H^+]}$$

$$H_3P^+ + H^+ \overset{K_2}{\rightleftharpoons} H_4P^{2+} \qquad K_2 = \frac{[H_4P^{2+}]}{[H_3P^+][H^+]}$$

β for **3** (1×10^5). Therefore, the first protonation is not significantly affected by ring-fusion. In sharp contrast, the second protonation constants, K_2, of **2**, **4**, and **5** decrease with increase in the number of fused rings. Stepwise protonation behavior is relatively rare for porphyrins,[7−9] because the first protonation of a porphyrin causes loss of the planarity, making the second protonation more feasible. On the other hand, the difficulty in the second protonation of the fused porphyrins can be explained by the rigidity of the porphyrin skeleton caused by the ring-fusion, which makes it harder to avoid the steric repulsion among the inner protons. As noted above, when normal porphyrins including **3** are diprotonated, the steric repulsion among the inner four protons results in saddle-type distortion of the porphyrin core by virtue of the structural flexibility.[5c,10c] On the other hand, the ring-fused porphyrins cannot strain enough to evade the steric repulsion among the inner protons, due to the structural rigidity gained by the ring-fusion. In fact, the DFT-optimized structures of the diprotonated forms for **2**, **4**, and **5** do not exhibit severe distortion of the porphyrin skeletons, compared to the structure of the diprotonated **3** (Figure 5a). Instead of distortion of the porphyrin core, the N−H bonds are warped to opposite directions to avoid the steric repulsion among the inner protons as observed in the optimized structures, which causes the instability of the diprotonated forms. For the monoprotonated forms of **2**, **4**, and **5**, the three inner protons are placed in the inner space of the porphyrin core without distortion of the porphyrin core and severe warp of the N−H bonds to suppress the steric repulsion (Figure 5b). Therefore, the first protonation constants for **2**, **4**, and **5** do not become significantly small due to the ring fusion.[46,47]

Redox Properties of Protonated QFP. To elucidate impacts of the protonation on redox potentials of freebase QFP, electrochemical studies of **2** were performed in the presence of TFA (Figure 6 and Table 2). The solubility of monoprotonated **2** (**2**-H^+) is low in CH_2Cl_2 containing 0.1 M tetrabutylammonium hexafluorophosphate as an electrolyte for electrochemical measurements, and thus, 0.1 M tetrabutylammonium tetraphenylborate ($TBABPh_4$) was used as an electrolyte. Due to utilization of $TBABPh_4$, the potential window of electrochemical measurements was narrowed on the anodic side and only reduction waves of the QFP derivatives are discussed in this study. A cyclic voltammogram of **2** in CH_2Cl_2 in the absence of acids exhibited quasi-reversible waves at −1.24 and −1.50 V vs Fc/Fc^+ (Figure 6a and d), which were assigned to the first and second reduction processes of **2**, respectively.

When the concentration of TFA was adjusted to be 1.3 mM in the solution of **2** (0.61 mM) in CH_2Cl_2, 99% of **2** in the solution was monoprotonated on the basis of the equilibrium constant described above and resultantly in a positive shift of the reduction potentials was observed; the first and second quasi-reversible waves of **2**-H^+ were observed at −0.89 and −1.15 V vs Fc/Fc^+ (Figure 6b and e). The potential shifts of the first and second redox processes were both +0.35 V, relative to those of **2**. Upon further addition of TFA to reach the concentration of 1 M, 87% of **2** in the solution was diprotonated; the first reduction potential was more positively shifted to −0.41 V vs Fc/Fc^+ (Figure 6c and f). The second reduction wave was not observed due to the fact that the potential window of the solution was narrowed by addition of excess TFA.

To elucidate the electronic structure of $1e^-$-reduced species of **2**-H^+, an ESR spectrum of electrochemically $1e^-$-reduced **2**-H^+ was measured in CH_2Cl_2 at 223 K (Figure 7). Controlled-potential bulk electrolysis of the CH_2Cl_2 solution of **2**-H^+ in the presence of $TBABPh_4$ (0.1 M) was performed at −1.0 V vs Ag/AgCl at 223 K. As a result, a clear ESR signal was observed at g = 2.003 with well-resolved hyperfine splitting in the ESR

Table 1. Equilibrium Constants for Protonation of 2, 3, 4, and 5 with TFA in CH_2Cl_2 at 298 K

compound	**2**	**3**	**4**	**5**
K_1, $10^5\ M^{-1}$	1.3 ± 0.1		1.1 ± 0.3	2.1 ± 0.2
K_2, M^{-1}	7.3 ± 0.3		(1.9 ± 0.3) × 10^2	(1.4 ± 0.2) × 10^2
β,[a] M^{-2}	(9.5 ± 1.1) × 10^5	(1.0 ± 0.3) × 10^{10}	(2.1 ± 1.0) × 10^6	(2.9 ± 0.7) × 10^7

[a] $\beta = K_1 \times K_2$.

DOI: 10.1021/acs.joc.6b02419
J. Org. Chem. 2017, 82, 322−330

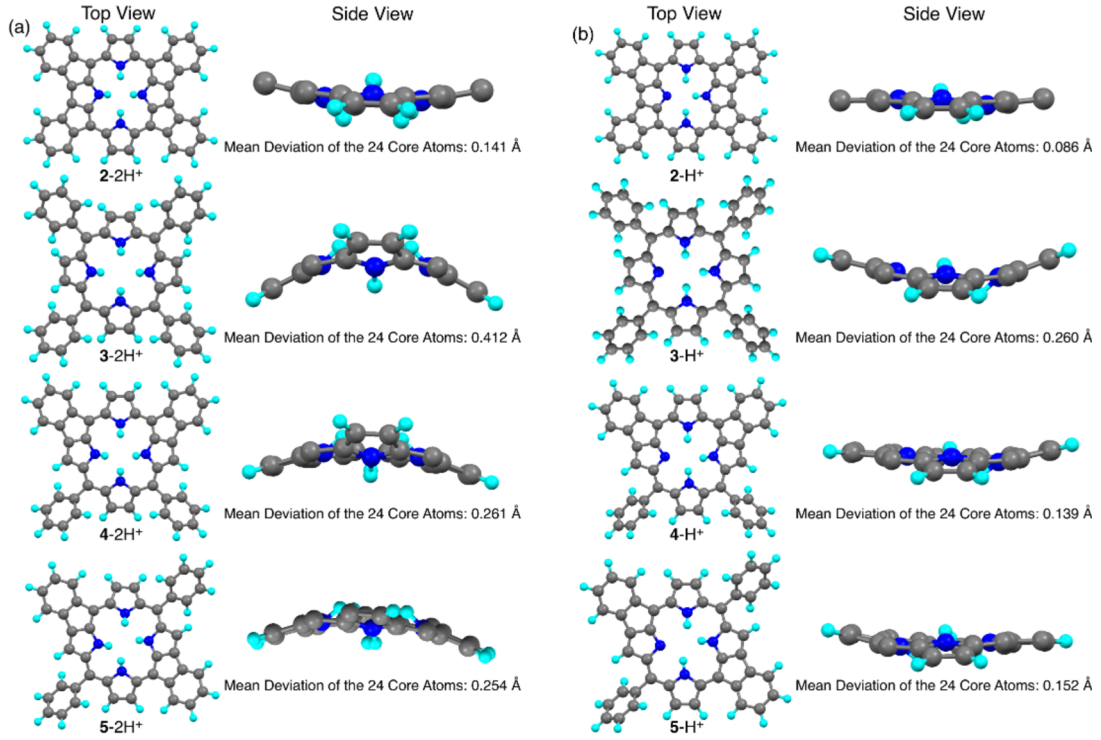

Figure 5. DFT-optimized structures of the diprotonated (a) and monoprotonated forms (b) of **2**, **3**, **4**, and **5**. The *t*-Bu groups were replaced with hydrogen atoms for computational costs. In the side views, the fused-phenyl moieties and phenyl groups at the *meso*-positions are omitted for clarity.

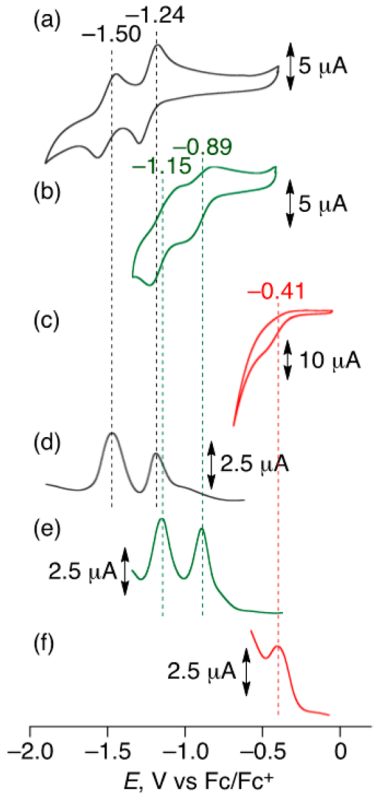

Figure 6. Cyclic (a, b, and c) and differential-pulse voltammograms (d, e, and f) of **2** (a and d), **2**-H^+ (b and e), and **2**-$2H^+$ (c and f) in CH_2Cl_2 in the presence of $TBABPh_4$ (0.1 M) at 298 K. The detailed procedures to form protonated species of **2** are described in the Experimental Section.

Table 2. Redox Potentials of 2 in its Various Protonated States in CH_2Cl_2 in the Presence of 0.1 M $TBABPh_4$ at 298 K

	E, V vs Fc/Fc^+	
	$P/P^{\cdot-}$	$P^{\cdot-}/P^{2-}$
2	−1.24	−1.50
2-H^+	−0.89	−1.15
2-$2H^+$	−0.41	

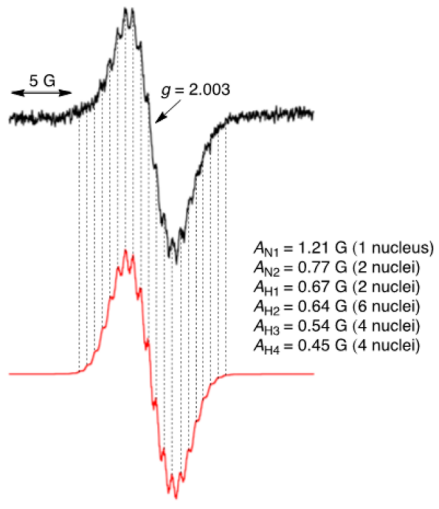

Figure 7. ESR spectrum (black line) of electrochemically $1e^-$-reduced **2**-H^+ in CH_2Cl_2 at 223 K in the presence of $TBABPh_4$ (0.1 M) and the simulated one (red line) with the hyperfine coupling constants.

spectrum (black trace in Figure 7). To investigate the spin distributions of the $1e^-$-reduced species of **2**-H^+, DFT calculations were performed at the UB3LYP/6-31+G** level

DOI: 10.1021/acs.joc.6b02419
J. Org. Chem. 2017, 82, 322−330

of theory. The spin-density distribution indicates that the unpaired electron localizes on three inner nitrogen atoms except the protonated fused pyrrole nitrogen atom (Figure 8).

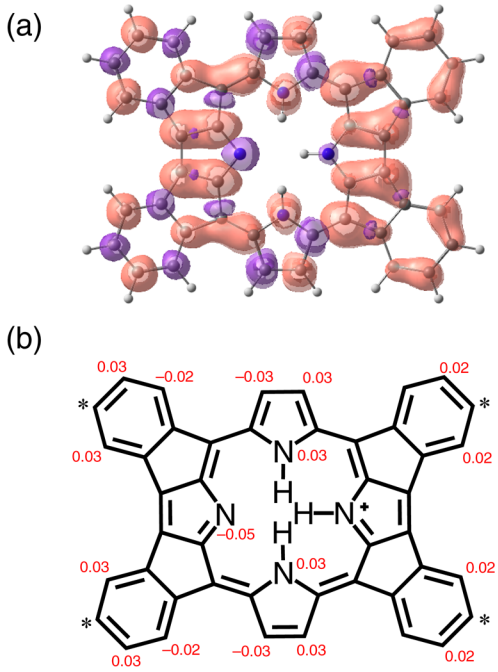

Figure 8. Spin density distribution (a) and schematic description of its spin densities (b) of the 1e$^-$-reduced species of **2**-H$^+$ obtained by DFT calculations at the UB3LYP/6-31+G** level of theory. The *t*-Bu groups of **2**-H$^+$ at the positions noted by asterisks (*) are replaced with hydrogen atoms for computational costs.

ESR simulation was performed (red trace in Figure 7) by considering contribution from hyperfine coupling with the three inner nitrogen nuclei and 16 protons attached to the two inner nitrogen, four pyrrole-*β*, and ten fused *meso*-aryl positions (Figure 8b). The simulated spectrum well reproduces the experimental result (Figure 7), and thus, the unsymmetrical electronic structure induced by the monoprotonation has been confirmed by the ESR measurement.

CONCLUSIONS

We have synthesized and characterized a freebase derivative of QFP, **2**. Particularly, the basicity of the inner imine nitrogen atoms in **2** was investigated by UV−vis titration in CH_2Cl_2 with TFA as an acid. As a result, the first protonation of **2** proceeds similarly to TPP derivatives, whereas the second protonation is hard to occur unless large excess amount of TFA is added. This difference stems from the fact that the monoprotonated form of **2** maintains a stable planar structure; on the contrary, the diprotonated structure is unstable due to the severe repulsion among the four inner protons in the rigid planar framework of H_2QFP. The stepwise protonation also causes stepwise positive shifts of the reduction potentials of the H_2QFP derivatives. In addition, unsymmetrical electronic structure of the monoprotonated QFP has been revealed by the ESR spectrum of its 1e$^-$-reduced species, which was formed by electrochemical reduction.

EXPERIMENTAL SECTION

General. Chemicals and solvents were used as received from commercial sources unless otherwise mentioned. CH_2Cl_2 used for the UV−vis spectral measurements was distilled over CaH_2 before use. Compounds **1**,[33b] **3**,[48] and 2,3,12,13-tetrabromo-tetrakis(*p*-*t*-Bu-phenyl)-porphyrin (**6**)[33b] were synthesized according to the literature procedure.

^{1}H NMR measurements were performed on 400, 500, and 600 MHz spectrometers. UV−vis absorption spectra were measured in CH_2Cl_2. MALDI-TOF-MS spectrometry was performed using dithranol as a matrix. Electrochemical experiments were done under an atmospheric pressure of Ar at 298 K with a CH_2Cl_2 solution of **2** (0.61 mM), with that of **2** (0.61 mM) including TFA (1.3 mM), in which 99% of **2** were monoprotonated, and with that of **2** (0.61 mM) including TFA (1 M), in which 87% of **2** were diprotonated. The aforementioned three solutions of **2** used for the electrochemical measurements contained $TBABPh_4$ (0.1 M) as an electrolyte. A small three-electrode cell (2.0 mL) was used with a gold-disk working electrode and a platinum wire as the counter electrode for the electrochemical measurements. The potentials were measured with respect to the Ag/AgCl reference electrode. Before the measurements, CV of ferrocene was measured to convert all of the potentials to values vs that of the ferrocene/ferrocenium redox couple. X-band ESR spectra were obtained on a spectrometer equipped with a temperature controller. To measure ESR spectra of the 1e$^-$-reduced species of **2**-H$^+$, electrochemical reduction of **2**-H$^+$ was performed in an ESR cell containing a CH_2Cl_2 solution of **2** (0.53 mM), TFA (1.0 mM) as an acid, and $TBABPh_4$ (0.1 M) as an electrolyte. The ESR cell was equipped with helix gold working electrode, gold wire as a counter electrode, and an Ag wire covered with AgCl as a reference electrode. The applied voltage was −1.0 V vs Ag/AgCl. The simulation of the ESR spectrum was carried out with use of the WinSIM software.[49]

Synthesis. *24,30,36,42-Tetrakis(tert-butyl)-Quadruply Fused Porphyrin (**2**).* To a solution of **1** (32.6 mg, 36.4 *μ*mol) in $CHCl_3$ (50 mL), was added TFA (6.0 mL, 78 mmol) and the reaction mixture was stirred for 1 h at room temperature. The reaction mixture was washed with Na_2CO_3 aq and water, and dried over Na_2SO_4. The solvent was removed under vacuum. The residual solid was recrystallized from CH_2Cl_2/EtOH (1:3, v/v) to give dark blue crystals of **2** (25.2 mg, 30.4 *μ*mol, 83%). ^{1}H NMR ($CDCl_3$, Figure S11): *δ* 7.51 (d, *J* = 1.6 Hz, 4H, 2,3,12,13-*β*-H), 6.88 (d, *J* = 7.4 Hz, 4H, 26,32,38,44-Ph-H), 6.68−6.65 (m, 8H, 23,29,35,41- Ph-H), 4.91 (br s, 2H, inner NH), 1.37 (s, 36H, *t*-Bu-CH_3). UV−vis (CH_2Cl_2): λ_{max} [nm] (log *ε*) = 817 (3.62), 742 (4.03), 663 (4.21), 604 (4.88), 478 (4.49), 416 (4.77), 331 (4.76). MS (MALDI-TOF, dithranol matrix): *m*/*z* = 831.9 (calcd. for [M]$^+$: 831.4). Anal. Calcd for $C_{60}H_{54}N_4 \cdot 0.5H_2O$: C 85.78, H 6.60, N 6.67; Found: C 85.83, H 6.71, N 6.47. mp >300 °C.

*24,30,36,42-Tetrakis(tert-butyl)-Doubly Fused Porphyrins (**4** and **5**).* A solution of tetra(*n*-butyl)ammonium acetate (TBA·OAc, 500 mg, 1.65 mmol), palladium acetate (10.5 mg, 46.6 *μ*mol), triphenylphosphine (20.8 mg, 79.1 *μ*mol), molecular sieves 4A (70 mg), potassium carbonate (552 mg, 3.99 mmol), and **6** (112 mg, 92 *μ*mol) in 1,4-dioxane (2 mL) was stirred at 110 °C for 16 h.[50] The reaction mixture was cooled to ambient temperature, filtered, and washed with water. The residual solid was dissolved in $CHCl_3$ (30 mL) and then filtered. To the filtrate was added TFA (3 mL, 39 mmol) and the reaction mixture was stirred for 3 h at room temperature. The reaction mixture was washed with Na_2CO_3 aq and water, and dried over Na_2SO_4. The solvent was removed under vacuum and the red-brown powder obtained was chromatographed on a silica gel column by using toluene/hexane (1:2, v/v) as an eluent and three fractions were obtained. Recrystallization of solids obtained from the second fraction from CH_2Cl_2/MeOH gave light-red powder of **4** (5.3 mg, 6.4 *μ*mol, 7%). Solids obtained from the first and the third fractions were recrystallized from the same solvent to give red powder of **5** (8.7 mg, 10.4 *μ*mol, 11%) and red powder of triply fused **7** (36.7 mg, 44.1 *μ*mol, 48%), respectively.

*24,30,36,42-Tetrakis(tert-butyl)-cis-Doubly Fused Porphyrin (**4**).* ^{1}H NMR ($CDCl_3$, 298 K, Figure S13): *δ* 8.61 (d, *J* = 1.6 Hz, 2H, 12,13-*β*-H), 7.78 (d, *J* = 8.3 Hz, 4H, 26,44-Ph-H), 7.66 (d, *J* = 1.9 Hz, 2H, 23,41-Ph-H), 7.63−7.59 (m, 6H, 2,3-*β*-H, *m*-Ph-H), 7.20 (s, 2H, 8,17-*β*-H), 7.04 (dd, *J* = 7.9, 1.9 Hz, 2H, 25,43-Ph-H), 5.30 (s, 1H,

DOI: 10.1021/acs.joc.6b02419
J. Org. Chem. 2017, 82, 322−330

inner NH), 2.86 (s, 1H, inner NH), 1.52 (s, 18H, *t*-Bu-CH_3), 1.35 (s, 18H, 24,42-*t*-Bu-CH_3). UV−vis (CH_2Cl_2): λ_{max} [nm] (log ε) = 309 (4.64), 417 (4.71), 496 (4.66), 534 (4.97), 577 (4.39), 693 (3.89), 771 (3.25). MS (MALDI-TOF, dithranol matrix): m/z = 835.1 (calcd. for $[M+H]^+$: 835.5). Anal. Calcd for $C_{60}H_{58}N_4 \cdot 1.5H_2O \cdot 0.5CH_2Cl_2$: C 80.33, H 6.91, N 6.19; Found: C 80.36, H 6.99, N 5.93. mp >300 °C.

*24,30,36,42-Tetrakis(tert-Butyl)-trans-Doubly Fused Porphyrin (**5**).* ^{1}H NMR ($CDCl_3$, 298 K, Figure S15): δ 8.69 (dd, J = 4.8, 2.0 Hz, 2H, 3,13-β-H), 8.26 (dd, J = 4.8, 2.0 Hz, 4H, 2,12-β-H), 7.87 (d, J = 8.2 Hz, 4H, *o*-Ph-H), 7.77 (d, J = 8.0 Hz, 2H, 32,44-Ph-H), 7.68 (d, J = 8.2 Hz, 4H, *m*-Ph-H), 7.38 (s, 2H, 7,17-β-H), 7.20 (d, J = 1.7 Hz, 2H, 29,41-Ph-H), 6.99 (dd, J = 8.0, 1.7 Hz, 2H, 31,43-Ph-H), 2.64 (s, 1H, inner NH), 1.34 (s, 36H, *t*-Bu-CH_3). UV−vis (CH_2Cl_2): λ_{max} [nm] (log ε) = 316 (4.69), 381 (4.43), 429 (4.74), 454 (4.69), 487 (5.10), 513 (3.71), 668 (4.91), 733 (3.97), 798 (3.64), 898 (3.60). MS (MALDI-TOF, dithranol matrix): m/z = 835.0 (calcd. for $[M+H]^+$: 835.5). Anal. Calcd for $C_{60}H_{58}N_4 \cdot 1.5H_2O \cdot CH_2Cl_2$: C 77.36, H 6.70, N 5.92; Found: C 77.19, H 6.61, N 5.74. mp >300 °C.

X-ray Diffraction Analysis. Recrystallization of **2** from the solution in chloroform with vapor deposition of acetonitrile as a poor solvent gave single crystals of **2**. A single crystal of **2** was mounted on a mounting loop. All diffraction data were collected at −153 °C equipped with graphite-monochromated Mo Kα (λ = 0.71073 Å) by the ω-2θ scan. The structures were solved by direct methods using SIR97 and SHELX-2013.[51] Crystallographic data for **2** are summarized in Table S1. CCDC-1434621 contains the supplementary crystallographic data. The cocrystallized chloroform molecules in the crystal of **2** were severely disordered and thus deleted by using the SQUEEZE program.[41] The disorder of cocrystallized solvent molecules caused weak diffraction in the high angle region, which resulted in the low value of sin2θ/λ (0.4674) relative to the IUCr criteria.

Determination of Equilibrium Constants of Protonation of the Fused Porphyrin Derivatives. A solution of a freebase porphyrin derivative was titrated with that of TFA in CH_2Cl_2 at 298 K and the absorbance change at an appropriate wavelength was fitted on the basis of eq 1 (Figure 4, and Figures S7 and S8).

$$\begin{aligned} \mathrm{Abs} = {} & \varepsilon_P[P]_0 + \{(\varepsilon_{HP} - \varepsilon_P)/(2 \times K)\} \\ & \times [(1 + K \times [TFA] + K \times [P]_0) \\ & - \{(1 + K \times [TFA] + K \times [P]_0)_2 - 4 \times K^2] \\ & \times [TFA] \times [P]_0\}^{1/2} \end{aligned} \quad (1)$$

Here, ε_P, $[P]_0$, [TFA], ε_{HP}, and K refer to the absorption coefficient of the porphyrin derivative at a certain wavelength, the concentration of the porphyrin derivative, the concentration of TFA added, the absorption coefficient of the associated complex between the porphyrin derivative and TFA at the corresponding wavelength, and the binding constant, respectively.

■ ASSOCIATED CONTENT

Supporting Information

The Supporting Information is available free of charge on the ACS Publications website at DOI: 10.1021/acs.joc.6b02419.

Details of DFT calculations, crystal packing, UV−vis spectral changes in titration experiments, resonance structures of the fused porphyrins, 1D and 2D ^{1}H NMR spectra (PDF)

X-ray crystallographic data for **2** (CIF)

■ AUTHOR INFORMATION

Corresponding Authors

*ishizuka@chem.tsukuba.ac.jp

*kojima@chem.tsukuba.ac.jp

ORCID

Takahiko Kojima: 0000-0001-9941-8375

Notes

The authors declare no competing financial interest.

■ ACKNOWLEDGMENTS

The authors thank Prof. Shigehisa Akine (Kanazawa University) for providing a nonlinear least-squares regression program. This work was supported by Grants-in-Aid (Nos. 22750118, 25410033, 16K05739, and 24245011) and a Grant-in-Aid for JSPS Fellows (16J05288 to Y.S.) from Japan Society for the Promotion of Science (JSPS).

■ REFERENCES

(1) (a) *The Porphyrin Handbook*, Vol. *1*−*10*; Kadish, K. M., Smith, K. M., Guilard, R., Eds.; Academic Press: New York, 2000. (b) Buchler, J. W. in *The Porphyrins*, Vol. *1*; Dolphin, D., Ed.; Academic Press: New York, 1979. (c) *Porphyrins and Metalloporphyrins*; Smith, K. M., Ed.; Elsevier: Amsterdam-Oxford, NY, 1975.

(2) (a) Kadish, K. M.; Guo, N.; Van Caemelbecke, E.; Froiio, A.; Paolesse, R.; Monti, D.; Tagliatesta, P.; Boschi, T.; Prodi, L.; Bolletta, F.; Zaccheroni, N. *Inorg. Chem.* **1998**, *37*, 2358. (b) Bhyrappa, P.; Krishnan, V. *Inorg. Chem.* **1991**, *30*, 239. (c) Shen, J.; Shao, J.; Ou, Z.; Koszarna, W. E. B.; Gryko, D. T.; Kadish, K. M. *Inorg. Chem.* **2006**, *45*, 2251. (d) Fang, Y.; Bhyrappa, P.; Ou, Z.; Kadish, K. M. *Chem. - Eur. J.* **2014**, *20*, 524. (e) Fang, Y.; Gorbunova, Y. G.; Chen, P.; Jiang, X.; Manowong, M.; Sinelshchikova, A. A.; Enakieva, Y. Y.; Martynov, A. G.; Tsivadze, A. Y.; Bessmertnykh-Lemeune, A.; Stern, C.; Guilard, R.; Kadish, K. M. *Inorg. Chem.* **2015**, *54*, 3501. (f) Rananaware, A.; Bhosale, R. S.; Ohkubo, K.; Patil, H.; Jones, L. A.; Jackson, S. L.; Fukuzumi, S.; Bhosale, S. V.; Bhosale, S. V. *J. Org. Chem.* **2015**, *80*, 3832.

(3) (a) Warren, J. J.; Winkler, J. R.; Gray, H. B. *Coord. Chem. Rev.* **2013**, *257*, 165. (b) Michel, H.; Deisenhofer, J. *Biochemistry* **1988**, *27*, 1. (c) Allen, J. P.; Feher, G.; Yeates, T. O.; Komiya, H.; Rees, D. C. *Proc. Natl. Acad. Sci. U. S. A.* **1987**, *84*, 5730. (d) Boxer, S. G. *Biochim. Biophys. Acta, Rev. Bioenerg.* **1983**, *726*, 265.

(4) (a) Wasielewski, M. R. *Chem. Rev.* **1992**, *92*, 435. (b) Gust, D.; Moore, T. A.; Moore, A. L. *Acc. Chem. Res.* **1993**, *26*, 198. (c) Guldi, D. M. *Chem. Soc. Rev.* **2002**, *31*, 22. (d) Osuka, A.; Marumo, S.; Mataga, N.; Taniguchi, S.; Okada, T.; Yamazaki, I.; Nishimura, Y.; Ohno, T.; Nozaki, K. *J. Am. Chem. Soc.* **1996**, *118*, 155. (e) Osuka, A.; Noya, G.; Taniguchi, S.; Okada, T.; Nishimura, Y.; Yamazaki, I.; Mataga, N. *Chem. - Eur. J.* **2000**, *6*, 33. (f) Kelson, M. M. A.; Bhosale, R. S.; Ohkubo, K.; Jones, L. A.; Bhosale, S. V.; Gupta, A.; Fukuzumi, S.; Bhosale, S. V. *Dyes Pigm.* **2015**, *120*, 340.

(5) (a) Hambright, P. *Coord. Chem. Rev.* **1971**, *6*, 247. (b) Aronoff, S. *J. Phys. Chem.* **1958**, *62*, 428. (c) Stone, A.; Fleischer, E. B. *J. Am. Chem. Soc.* **1968**, *90*, 2735. (d) Karaman, R.; Bruice, T. C. *Inorg. Chem.* **1992**, *31*, 2455. (e) Sutter, T. P. C.; Hambright, P. *Inorg. Chem.* **1992**, *31*, 5089.

(6) (a) Braun, J.; Hasenfratz, C.; Schwesinger, R.; Limbach, H.-H. *Angew. Chem., Int. Ed. Engl.* **1994**, *33*, 2215. (b) Barrett, A. J.; Kennedy, J. C.; Jones, R. A.; Nadeau, P.; Pottier, R. *J. Photochem. Photobiol., B* **1990**, *6*, 309.

(7) (a) Hrung, C. P.; Tsutsui, M.; Cullen, D. L.; Meyer, E. F., Jr. *J. Am. Chem. Soc.* **1976**, *98*, 7878. (b) Hrung, C. P.; Tsutsui, M.; Cullen, D. L.; Meyer, E. F., Jr.; Morimoto, C. N. *J. Am. Chem. Soc.* **1978**, *100*, 6068.

(8) (a) Ogoshi, H.; Watanabe, E.; Yoshida, Z. *Tetrahedron* **1973**, *29*, 3241. (b) Almarsson, Ö.; Blasko, A.; Bruice, T. C. *Tetrahedron* **1993**, *49*, 10239.

(9) (a) De Luca, G.; Romeo, A.; Monsù Scolaro, L.; Ricciardi, G.; Rosa, A. *Inorg. Chem.* **2007**, *46*, 5979. (b) Thyagarajan, S.; Leiding, T.; Peterson Årsköld, S.; Cheprakov, A. V.; Vinogradov, S. A. *Inorg. Chem.* **2010**, *49*, 9909. (c) Honda, T.; Kojima, T.; Fukuzumi, S. *Chem. Commun.* **2009**, 4994. (d) Rudine, A. B.; Del Fatti, B. D.; Wamser, C. C. *J. Org. Chem.* **2013**, *78*, 6040.

(10) (a) Senge, M. O.; Forsyth, T. P.; Nguyen, L. T.; Smith, K. M. *Angew. Chem., Int. Ed. Engl.* **1995**, *33*, 2485. (b) Meot-Ner, M.; Adler,

A. D. *J. Am. Chem. Soc.* **1975**, *97*, 5107. (c) Cheng, B.; Munro, O. Q.; Marques, H. M.; Scheidt, W. R. *J. Am. Chem. Soc.* **1997**, *119*, 10732.
(11) (a) Stepanek, P.; Andrushchenko, V.; Ruud, K.; Bour, P. *J. Phys. Chem. A* **2012**, *116*, 778. (b) Rudine, A. B.; DelFatti, B. D.; Wamser, C. C. *J. Org. Chem.* **2013**, *78*, 6040. (c) Rosa, A.; Ricciardi, G.; Jan Baerends, E.; Romeo, A.; Monsù Scolaro, L. *J. Phys. Chem. A* **2003**, *107*, 11468.
(12) (a) Chirvony, V. S.; van Hoek, A.; Galievsky, V. A.; Sazanovich, I. V.; Schaafsma, T. J.; Holten, D. *J. Phys. Chem. B* **2000**, *104*, 9909. (b) Stepánek, P.; Andrushchenko, V.; Ruud, K.; Bour, P. *J. Phys. Chem. A* **2012**, *116*, 778.
(13) (a) Langhus, D. L.; Wilson, G. S. *Anal. Chem.* **1979**, *51*, 1139. (b) Ojadi, E. C. A.; Linschitz, H.; Gouterman, M.; Walter, R. I.; Lindsey, J. S.; Wagner, R. W.; Droupadi, P. R.; Wang, W. *J. Phys. Chem.* **1993**, *97*, 13192.
(14) (a) Pasternack, R. F.; Huber, P. R.; Boyd, P.; Engasser, G.; Francesconi, L.; Gibbs, E.; Fasella, P.; Cerio Venturo, G.; Hinds, L. *J. Am. Chem. Soc.* **1972**, *94*, 4511. (b) Kadish, K. M.; Maiya, G. B.; Araullo, C.; Guilard, R. *Inorg. Chem.* **1989**, *28*, 2725. (c) Barber, D. C.; Freitag-Beeston, R. A.; Whitten, D. G. *J. Phys. Chem.* **1991**, *95*, 4074.
(15) (a) De Luca, G.; Romeo, A.; Monsù Scolaro, L. *J. Phys. Chem. B* **2005**, *109*, 7149. (b) De Luca, G.; Romeo, A.; Monsù Scolaro, L. *J. Phys. Chem. B* **2006**, *110*, 7309. (c) De Luca, G.; Romeo, A.; Monsù Scolaro, L. *J. Phys. Chem. B* **2006**, *110*, 14135.
(16) (a) Fukuzumi, S.; Honda, T.; Kojima, T. *Coord. Chem. Rev.* **2012**, *256*, 2488 and references therein. (b) Kojima, T.; Honda, T.; Ohkubo, K.; Shiro, M.; Kusukawa, T.; Fukuda, T.; Kobayashi, N.; Fukuzumi, S. *Angew. Chem., Int. Ed.* **2008**, *47*, 6712. (c) Nakanishi, T.; Ohkubo, K.; Kojima, T.; Fukuzumi, S. *J. Am. Chem. Soc.* **2009**, *131*, 577.
(17) Reviews on this topic: (a) Fox, S.; Boyle, R. W. *Tetrahedron* **2006**, *62*, 10039. (b) Lewtak, J. P.; Gryko, D. T. *Chem. Commun.* **2012**, *48*, 10069. (c) Mori, H.; Tanaka, T.; Osuka, A. *J. Mater. Chem. C* **2013**, *1*, 2500. (d) Stępień, M.; Gońka, E.; Żyła, M.; Sprutta, N. *Chem. Rev.* **2016**, DOI: 10.1021/acs.chemrev.6b00076.
(18) (a) Edwards, L.; Gouterman, M.; Rose, C. B. *J. Am. Chem. Soc.* **1976**, *98*, 7638. (b) Lash, T. D.; Novak, B. H. *Angew. Chem., Int. Ed. Engl.* **1995**, *34*, 683. (c) Ito, S.; Murashima, T.; Uno, H.; Ono, N. *Chem. Commun.* **1998**, 1661.
(19) (a) Deshpande, R.; Jiang, L.; Schmidt, G.; Rakovan, J.; Wang, X.; Wheeler, K.; Wang, H. *Org. Lett.* **2009**, *11*, 4251. (b) Jiang, L.; Engle, J. T.; Sirk, L.; Hartley, C. S.; Ziegler, C. J.; Wang, H. *Org. Lett.* **2011**, *13*, 3020. (c) Banala, S.; Rühl, T.; Wurst, K.; Kräutler, B. *Angew. Chem., Int. Ed.* **2009**, *48*, 599.
(20) (a) Aihara, H.; Jaquinod, L.; Nurco, D. J.; Smith, K. M. *Angew. Chem., Int. Ed.* **2001**, *40*, 3439. (b) Nath, M.; Huffman, J. C.; Zaleski, J. M. *J. Am. Chem. Soc.* **2003**, *125*, 11484. (c) Nath, M.; Pink, M.; Zaleski, J. M. *J. Am. Chem. Soc.* **2005**, *127*, 478.
(21) (a) Cammidge, A. N.; Scaife, P. J.; Berber, G.; Hughes, D. L. *Org. Lett.* **2005**, *7*, 3413. (b) Tanaka, M.; Hayashi, S.; Eu, S.; Umeyama, T.; Matano, Y.; Imahori, H. *Chem. Commun.* **2007**, 2069. (c) Jiao, C.; Huang, K.-W.; Guan, Z.; Xu, Q.-H.; Wu, J. *Org. Lett.* **2010**, *12*, 4046.
(22) (a) Gill, H. S.; Harmjanz, M.; Santamaría, J.; Finger, I.; Scott, M. J. *Angew. Chem., Int. Ed.* **2004**, *43*, 485. (b) Kurotobi, K.; Kim, K. S.; Noh, S. B.; Kim, D.; Osuka, A. *Angew. Chem., Int. Ed.* **2006**, *45*, 3944.
(23) Jiao, C.; Zhu, L.; Wu, J. *Chem. - Eur. J.* **2011**, *17*, 6610.
(24) (a) Davis, N. K. S.; Pawlicki, M.; Anderson, H. L. *Org. Lett.* **2008**, *10*, 3945. (b) Davis, N. K. S.; Thompson, A. L.; Anderson, H. L. *Org. Lett.* **2010**, *12*, 2124. (c) Davis, N. K. S.; Thompson, A. L.; Anderson, H. L. *J. Am. Chem. Soc.* **2011**, *133*, 30.
(25) (a) Sendt, K.; Johnston, L. A.; Hough, W. A.; Crossley, M. J.; Hush, N. S.; Reimers, J. R. *J. Am. Chem. Soc.* **2002**, *124*, 9299. (b) Paolesse, R.; Jaquinod, L.; Della Sala, F.; Nurco, D. J.; Prodi, L.; Montalti, M.; Di Natale, C.; D'Amico, A.; Di Carlo, A.; Lugli, P.; Smith, K. M. *J. Am. Chem. Soc.* **2000**, *122*, 11295. (c) Uno, H.; Masumoto, A.; Ono, N. *J. Am. Chem. Soc.* **2003**, *125*, 12082. (d) Akita, M.; Hiroto, S.; Shinokubo, H. *Angew. Chem., Int. Ed.* **2012**, *51*, 2894.
(26) (a) Tsuda, A.; Nakano, A.; Furuta, H.; Yamochi, H.; Osuka, A. *Angew. Chem., Int. Ed.* **2000**, *39*, 558. (b) Tsuda, A.; Furuta, H.; Osuka, A. *Angew. Chem., Int. Ed.* **2000**, *39*, 2549. (c) Tsuda, A.; Furuta, H.; Osuka, A. *J. Am. Chem. Soc.* **2001**, *123*, 10304. (d) Tsuda, A.; Osuka, A. *Science* **2001**, *293*, 79. (e) Nakamura, Y.; Aratani, N.; Shinokubo, H.; Takagi, A.; Kawai, T.; Matsumoto, T.; Yoon, Z. S.; Kim, D. Y.; Ahn, T. K.; Kim, D.; Muranaka, A.; Kobayashi, N.; Osuka, A. *J. Am. Chem. Soc.* **2006**, *128*, 4119.
(27) (a) Woodward, R. B.; Ayer, W. A.; Beaton, J. M.; Bickelhaupt, F.; Bonnett, R.; Buchschacher, P.; Closs, G. L.; Dutler, H.; Hannah, J.; Hauck, F. P.; Ito, S.; Langemann, A.; Le Goff, E.; Leimgruber, W.; Lwowski, W.; Sauer, J.; Valenta, Z.; Volz, H. *J. Am. Chem. Soc.* **1960**, *82*, 3800. (b) Woodward, R. B.; Ayer, W. A.; Beaton, J. M.; Bickelhaupt, F.; Bonnett, R.; Buchschacher, P.; Closs, G. L.; Dutler, H.; Hannah, J.; Hauck, F. P.; Ito, S.; Langemann, A.; Le Goff, E.; Leimgruber, W.; Lwowski, W.; Sauer, J.; Valenta, Z.; Volz, H. *Tetrahedron* **1990**, *46*, 7599.
(28) (a) Fox, S.; Boyle, R. W. *Chem. Commun.* **2004**, 1322. (b) Shen, D.-M.; Liu, C.; Chen, Q.-Y. *Chem. Commun.* **2005**, 4982. (c) Shen, D.-M.; Liu, C.; Chen, Q.-Y. *J. Org. Chem.* **2006**, *71*, 6508.
(29) (a) Hayashi, S.; Matsubara, Y.; Eu, S.; Hayashi, H.; Umeyama, T.; Matano, Y.; Imahori, H. *Chem. Lett.* **2008**, *37*, 846. (b) Lash, T. D.; Smith, B. E.; Melquist, M. J.; Godfrey, B. A. *J. Org. Chem.* **2011**, *76*, 5335. (c) Pereira, A. M. V. M; Neves, M. G. P. M. S.; Cavaleiro, J. A. S.; Jeandon, C.; Gisselbrecht, J.-P.; Choua, S.; Ruppert, R. *Org. Lett.* **2011**, *13*, 4742.
(30) (a) Mitsushige, Y.; Yamaguchi, S.; Lee, B. S.; Sung, Y. M.; Kuhri, S.; Schierl, C. A.; Guldi, D. M.; Kim, D.; Matsuo, Y. *J. Am. Chem. Soc.* **2012**, *134*, 16540. (b) Fliegl, H.; Özcan, N.; Mera-Adasme, R.; Pichierri, F.; Jusélius, J.; Sundholm, D. *Mol. Phys.* **2013**, *111*, 1364.
(31) (a) Nakano, A.; Aratani, N.; Furuta, H.; Osuka, A. *Chem. Commun.* **2001**, 1920. (b) Sahoo, A. K.; Mori, S.; Shinokubo, H.; Osuka, A. *Angew. Chem., Int. Ed.* **2006**, *45*, 7972. (c) Fukui, N.; Yorimitsu, H.; Lim, J. M.; Kim, D.; Osuka, A. *Angew. Chem., Int. Ed.* **2014**, *53*, 4395.
(32) (a) Fukui, N.; Cha, W.-Y.; Lee, S.; Tokuji, S.; Kim, D.; Yorimitsu, H.; Osuka, A. *Angew. Chem., Int. Ed.* **2013**, *52*, 9728. (b) Ota, K.; Tanaka, T.; Osuka, A. *Org. Lett.* **2014**, *16*, 2974.
(33) (a) Ishizuka, T.; Saegusa, Y.; Shiota, Y.; Ohtake, K.; Yoshizawa, K.; Kojima, T. *Chem. Commun.* **2013**, *49*, 5939. (b) Saegusa, Y.; Ishizuka, T.; Komamura, K.; Shimizu, S.; Kotani, H.; Kobayashi, N.; Kojima, T. *Phys. Chem. Chem. Phys.* **2015**, *17*, 15001. (c) Saegusa, Y.; Ishizuka, T.; Kojima, T.; Mori, S.; Kawano, M.; Kojima, T. *Chem. - Eur. J.* **2015**, *21*, 5302.
(34) See the Supporting Information.
(35) In the case of tetraphenylporphyrin, only when the ^{1}H NMR spectrum was measured at very low temperature, where the inner NH protons localized at two pyrroles among four at the NMR timescale, splitting of the ^{1}H NMR signal assigned to the inner NH protons was observed due to the coupling of the ^{1}H NMR signal of the pyrrole β-protons: Storm, C. B.; Teklu, Y. *J. Am. Chem. Soc.* **1972**, *94*, 1745. Therefore, the splitting of the ^{1}H NMR signal due to the inner NH protons of **2** is a strong evidence to support that the inner NH protons localize at the non-fused pyrroles.
(36) Even at low temperature, the ^{1}H NMR signal of the inner NH protons did not show splitting due to formation of the other NH tautomer having the NH protons at the fused pyrroles (Figure S1).
(37) Lu, G.; Zhang, X.; Cai, X.; Fang, Y.; Zhu, M.; Zhu, W.; Ou, Z.; Kadish, K. M. *J. Porphyrins Phthalocyanines* **2013**, *17*, 941.
(38) The symbol of (1) represents that the NICS values are estimated at 1 Å above from the π-conjugated planes. (a) von Ragué Schleyer, P.; Maerker, C.; Dransfeld, A.; Jiao, H.; van Eikema Hommes, N. J. R. *J. Am. Chem. Soc.* **1996**, *118*, 6317. (b) Gomes, J. A. N. F.; Mallion, R. B. *Chem. Rev.* **2001**, *101*, 1349.
(39) Downfield shifts of the inner NH signals due to the strong hydrogen bonds were also observed for porphycene (ν_{NH} = 3099 cm^{-1}), and the ^{1}H NMR signal of the inner NHs for porphycene appeared at 3.24 ppm in $CDCl_3$. See: Vogel, E.; Kocher, M.; Schmickler, H.; Lex, J. *Angew. Chem., Int. Ed. Engl.* **1986**, *25*, 257.

DOI: 10.1021/acs.joc.6b02419
J. Org. Chem. 2017, 82, 322−330

(40) Braun, J.; Schlabach, M.; Wehrle, B.; Köcher, M.; Vogel, E.; Limbach, H.-H. *J. Am. Chem. Soc.* **1994**, *116*, 6593.
(41) van der Sluis, P.; Spek, A. L. *Acta Crystallogr., Sect. A: Found. Crystallogr.* **1990**, *46*, 194.
(42) (a) Silvers, S. J.; Tulinsky, A. *J. Am. Chem. Soc.* **1967**, *89*, 3331. (b) Jameson, G. B.; Ibers, J. A. *J. Am. Chem. Soc.* **1980**, *102*, 2823.
(43) One might consider that this difference in Cα-N-Cα bond angles between the fused and nonfused pyrroles derives from the structural requirement by the ring fusion; however, the Cα−N−Cα bond angles of the fused and nonfused pyrroles are almost the same in the QFP metal complexes (see ref 33). Therefore, the difference in the Cα−N−Cα bond angles is probably ascribable to the presence or absence of a proton at the pyrrole nitrogen atom.
(44) Pine, S. H.; *Organic Chemistry*, 5th ed.; McGraw-Hill: New York, 1987.
(45) Atkins, P.; de Paula, J. *Physical Chemistry*, 8th ed.; Oxford University Press: Oxford, 2006.
(46) During the reviewing process, one of the reviewers pointed out the possibility of self-aggregation of **2** and its protonated species in the solution; however, the absorption maxima are independent of the concentration (Figure S10), and thus, we conclude that compound **2** and its protonated species do not exhibit self-aggregation under the conditions examined.
(47) (a) Bobe, M. S. R.; Al Kobaisi, M.; Bhosale, S. V.; Bhosale, S. V. *ChemistryOpen* **2015**, *4*, 516. (b) Bhosale, S. V.; Nalage, S. V.; Booth, J. M.; Gupta, A.; Bhargava, S. K.; Bhosale, S. V. *Supramol. Chem.* **2012**, *24*, 779.
(48) Richeter, S.; Hadj-Aïssa, A.; Taffin, C.; van der Lee, A.; Leclercq, D. *Chem. Commun.* **2007**, 2148.
(49) The WinSIM program is developed at the NIEHS by Duling (URL: http://www.niehs.nih.gov/research/resources/software/tools/index).
(50) Higashibayashi, S.; Sakurai, H. *Chem. Lett.* **2007**, *36*, 18.
(51) Sheldrick, G. M. *SIR97 and SHELX97, Programs for Crystal Structure Refinement*; University of Göttingen: Göttingen, Germany, 1997.

DOI: 10.1021/acs.joc.6b02419
J. Org. Chem. 2017, 82, 322−330